Influence of air diffusion on the OH radicals and atomic O distribution in an atmospheric Ar (bio)plasma jet



2014 Plasma Sources Sci. Technol. 23 015015

(http://iopscience.iop.org/0963-0252/23/1/015015)

IOP Publishing Plasma Sources Science and Technology

Plasma Sources Sci. Technol. **23** (2014) 015015 (11pp) doi:10.1088/0963-0252/23/1/015015

# Influence of air diffusion on the OH radicals and atomic O distribution in an atmospheric Ar (bio)plasma jet

**A Nikiforov[1,2], L Li[1], N Britun[3], R Snyders[3,4], P Vanraes[1] and C Leys[1]**

[1] Department of Applied Physics, Research Unit Plasma Technology, Ghent University, Jozef Plateaustraat 22, Ghent B-9000, Belgium
[2] Institute of Solution Chemistry of the Russian Academy of Science, Academicheskaya St., 1, Ivanono, 153045, Russia
[3] Chimie des Interactions Plasma-Surface (ChIPS), CIRMAP, Universite de Mons, 20 Place du Parc, B-7000 Mons, Belgium
[4] Materia Nova Research Centre, Parc Initialis, B-7000 Mons, Belgium

E-mail: anton.nikiforov@ugent.be

Received 24 July 2013, revised 25 November 2013
Accepted for publication 28 November 2013
Published 4 February 2014

**Abstract**

Treatment of samples with plasmas in biomedical applications often occurs in ambient air. Admixing air into the discharge region may severely affect the formation and destruction of the generated oxidative species. Little is known about the effects of air diffusion on the spatial distribution of OH radicals and O atoms in the afterglow of atmospheric-pressure plasma jets. In our work, these effects are investigated by performing and comparing measurements in ambient air with measurements in a controlled argon atmosphere without the admixture of air, for an argon plasma jet. The spatial distribution of OH is detected by means of laser-induced fluorescence diagnostics (LIF), whereas two-photon laser-induced fluorescence (TALIF) is used for the detection of atomic O. The spatially resolved OH LIF and O TALIF show that, due to the air admixture effects, the reactive species are only concentrated in the vicinity of the central streamline of the afterglow of the jet, with a characteristic discharge diameter of ~1.5 mm. It is shown that air diffusion has a key role in the recombination loss mechanisms of OH radicals and atomic O especially in the far afterglow region, starting up to ~4 mm from the nozzle outlet at a low water/oxygen concentration. Furthermore, air diffusion enhances OH and O production in the core of the plasma. The higher density of active species in the discharge in ambient air is likely due to a higher electron density and a more effective electron impact dissociation of $H_2O$ and $O_2$ caused by the increasing electrical field, when the discharge is operated in ambient air.

Keywords: plasma jet, OH and O radicals, atmospheric plasma, laser-induced fluorescence, LIF, TALIF

(Some figures may appear in colour only in the online journal)

## 1. Introduction

One of the attractive features of a non-thermal atmospheric-pressure plasma is the ability to produce a large amount of reactive species without the need for elevated gas temperatures [1, 2]. Since the gas temperature in an atmospheric-pressure plasma remains relatively low, the plasma does not cause any thermal damage to the sensitive surface it comes in contact with. These properties make this type of plasma attractive for medical applications such as electrosurgery [3], tissue engineering [4] and surface modification of biocompatible materials [5]. Plasma jets in particular are playing an increasingly important role in various biomedical applications, because they provide plasmas that are not spatially bound or confined by high-voltage electrodes, allowing safer and more versatile use.

 

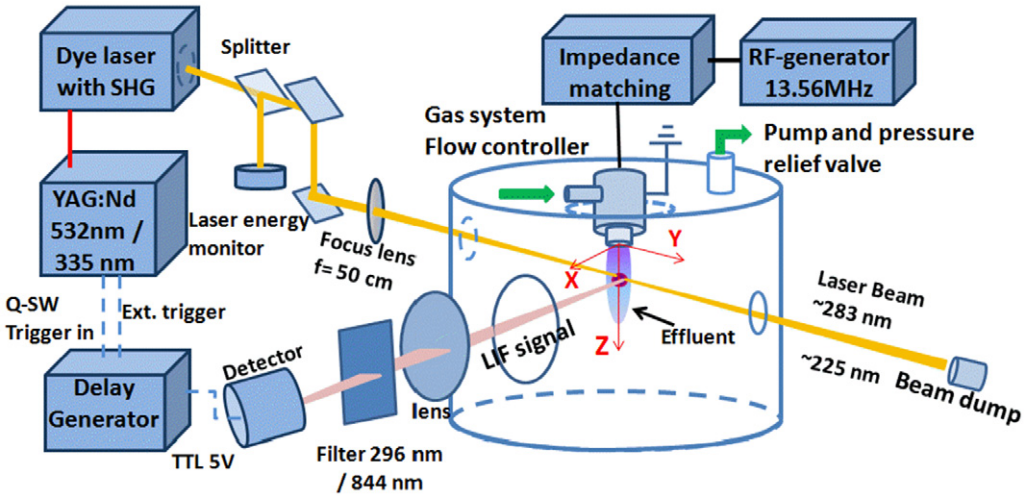


**Figure 1.** Schematic of the experimental apparatus used for the measurement of OH radicals and atomic O in the atmospheric-pressure RF plasma jet.

In many atmospheric-pressure plasma jets (APPJs), the plasma is generated in a noble gas with a small molecular component in order to produce strongly oxidizing species (OH, NO, NH, CH, O, H radicals, etc)—depending on the application under consideration [6, 7]. For medical applications, the highly reactive hydroxyl radical and atomic oxygen play a key role. For process efficiency, not only the yield of reactive species is important, since they also need to survive sufficiently long to be chemically active in the location required by the application. Therefore, the determination of active species concentration and its spatial distribution are of great interest. Moreover, a biomedical plasma is commonly used to treat samples in ambient air. Operating the discharge in direct contact with air makes the plasma vulnerable to intrusions of nitrogen and oxygen molecules from the surrounding environment. Thus, the effect of admixing air into the discharge may severely affect the formation, destruction and spatial distribution of the oxidative species.

In this paper, the spatial distribution of OH radicals and atomic O in a radio frequency (RF) plasma jet, operated in a chamber with controlled atmosphere and in ambient air, respectively, is determined by laser-induced fluorescence (LIF) spectroscopy. The main purpose of this work is to analyze the influence of ambient air on the spatial distribution of active species generated in the discharge.

## 2. Experimental set-up

A schematic diagram of the system used in this work is presented in figure 1, showing in particular the laser beam direction. The exciting UV laser beam is focused into a chamber which encloses the plasma jet. Throughout the experiments a total pressure of 1010 mbar is maintained in the chamber through a pressure relief valve. The capacitively coupled plasma jet is sustained in ambient argon and in ambient air, respectively. The design of the jet includes a centered RF (13.5 MHz) electrode in a quartz capillary with 2 mm inner diameter, surrounded by the cylindrical ground electrode. The voltage, current root mean square (RMS) values and operation voltage are obtained by connecting a Tektronix P5100 HV probe and Pearson-2877 current transformer in the L-matching impedance box right before the coil. The RF plasma jet is operated at a gas flow of 2 slm (standard liter per minute) of argon with a small admixture of water or oxygen (varying from 0.1% to 0.5%) at the input power of 15 W. The addition of $H_2O$ is used to enhance the production of OH radicals, whereas mixing a small amount of $O_2$ into the feed gas allows the generation of atomic oxygen. The laser spectroscopy system consists of a Nd : YAG laser pumping the Sirah Cobra-Stretch dye laser with a second harmonic generation unit. UV radiation around 283 nm is used to excite the ground-state OH radicals ($X\,^2\Pi$, $v'' = 0$) to the ($A\,^2\sum^+$, $v' = 1$). Deep UV light around 225 nm is applied for two-photon laser spectroscopy of atomic oxygen. The laser energy per pulse is kept in the range 10–20 $\mu$J for OH radical detection and around 0.4 mJ for atomic oxygen detection. The energy is monitored by an Ophir PE-9 energy measurement head. After passing through a bandpass filter, the fluorescence signal is detected by an Andor iStar 740 ICCD camera, which is synchronized with the laser pulse. The filter for OH detection has a maximal transparency around the wavelength of 309 nm, while the filter for oxygen detection is optimized to a wavelength of 844 nm, corresponding to the transition: $3p\ ^3P_2 \rightarrow 3s\ ^3S$. During all the measurements, the ICCD camera is operated in accumulation mode, using accumulations of 30 laser pulses. A two-dimensional axial map of LIF and two-photon laser-induced fluorescence (TALIF) is obtained by moving the laser beam in relation to the plasma jet. The spatial resolution of the system in the axial direction (defined as the $z$-axis in figure 1) is about 1 mm. All images are corrected for background light and subtraction of the discharge emission.

With $Ar/H_2O$ or $Ar/O_2$ as inlet gas mixtures, the spatial distribution of OH radicals and O atoms in the plasma jet is measured by means of LIF and TALIF spectroscopy, respectively. The principle of the used techniques is shown in figure 2. OH radicals are excited by single photon

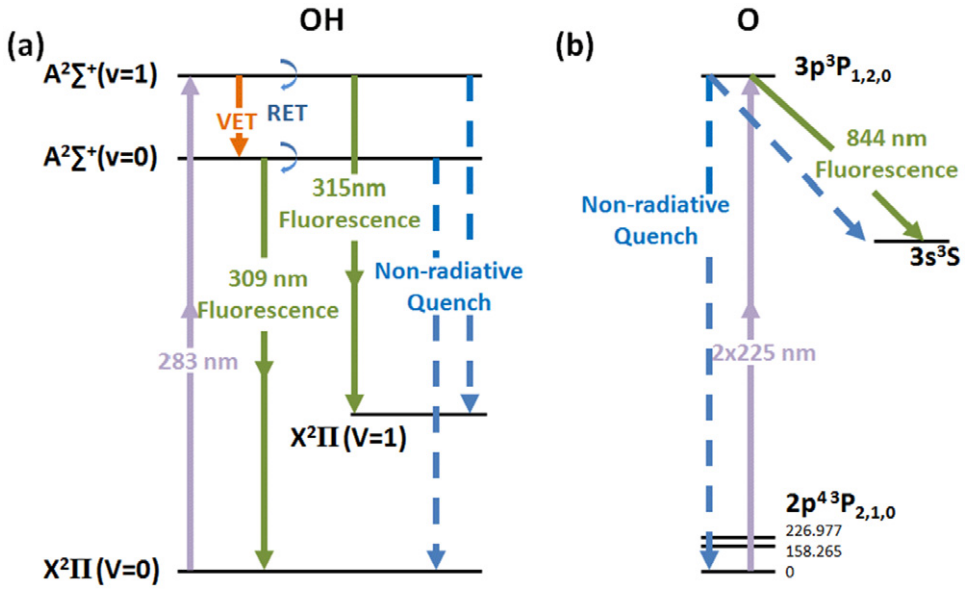


**Figure 2.** Schematic diagram of laser excitation and energy transfer processes of the (*a*) LIF and (*b*) TALIF experiments.

absorption, whereas absorption of two photons is required for the excitation of atomic oxygen from its ground state. The measurement configuration is similar to the one used in our recent works [8–11]. For the excitation of OH radicals, the electronic transition $A\,^2\sum - X\,^2\Pi$ is conventionally used via the transitions ($v'' = 0$, $v' = 0$) at 308 nm, (0, 1) at 283 nm and (3, 0) at 248 nm [8, 12–14]. The use of the resonance transition at 308 nm for LIF measurements is complicated due to the additional process of radiation reabsorption. Deep UV excitation at the vibrational level ($v'' = 3$, $v' = 0$) around 248 nm has a drawback of the strong interference of OH excitation by the process of $O_3$ photo-dissociation with the follow-up generation of OH radicals due to reactions involving atomic oxygen. Hence, the ($v'' = 0$, $v' = 1$) transition at 283 nm is utilized in the present work. For the TALIF experiments, the laser wavelength is fixed at 225.654 nm corresponding to the two-photon excitation energy gap (i.e. 112.827 nm) between the fine levels ($2p^4\ ^3P_2 \rightarrow 3p\ ^3P_2$) of O.

The LIF mechanism of OH excitation can be described as a two-step process. First, the OH radical in the ground state $\langle 1\rangle$ is excited by a laser photon to level $\langle 3\rangle$. Then, the excited OH radical relaxes by spontaneous emission, fluorescence, to a lower state $\langle 2\rangle$. The total emitted fluorescence radiation after a laser pulse is proportional to the ground-state density $N_{\mathrm{OH}}$. The spectrally and temporally integrated fluorescence signal intensity can be written as [10]

$$I_{\mathrm{LIF}} = G\Omega_{\mathrm{LIF}} V_{\mathrm{LIF}} \sum_l \left( \sum_m \frac{A_{lm}\varepsilon_{lm}t_{lm}}{4\pi} \int_0^\infty n_l \,\mathrm{d}t \right) \qquad (1)$$

where $G$ is the efficiency of the optical system, $\Omega_{\mathrm{LIF}}$ and $V_{\mathrm{LIF}}$ are the detection system's solid angle and the light-emitting volume, $\varepsilon_{lm}$ is the energy gap of the corresponding transition from rotational level $l$ of state $\langle 3\rangle$ to level $m$ of state $\langle 2\rangle$, $n_l$ is the density of radicals on the corresponding rotational level, and $t_{lm}$ is the corresponding filter transmittance. $A_{lm}$ is the sum of the radiative emission coefficient over all involved excited states. It is reasonable to write the summation of the upper state population over all involved rotational levels $l$ as

$$\sum_l (Q_l + A_l) \int_0^\infty n_l \,\mathrm{d}t = N_{\mathrm{OH}} B_{xl} \int_0^\infty I_{\mathrm{L}} \,\mathrm{d}t \qquad (2)$$

where $Q_l$ is the quenching rate of OH($A$) due to collision with Ar, $O_2$, $N_2$ and $H_2O$. $I_{\mathrm{L}}$ is the laser intensity, $B_{xi}$ is the rate of absorption. Thus, the calibrated LIF signal intensity $I^0_{\mathrm{LIF}}$ can be expressed as a function of $N_{\mathrm{OH}}$ as

$$I^0_{\mathrm{LIF}} = \eta N_{\mathrm{OH}} B_{xl} \int_0^\infty I_{\mathrm{L}} \,\mathrm{d}t \qquad (3)$$

where $\eta$ is the fluorescence yield, which represents the ratio of the molecules depopulated to the level $\langle 2\rangle$ due to fluorescence to the total number of laser-excited molecules. At atmospheric pressure, the collisional quenching significantly reduces the entire fluorescence signal, and non-radiative depopulation due to collisional quenching of the laser-excited levels is taken into account through the fluorescence yield $\eta$,

$$\eta = \frac{\sum_{ik} A_{ik}}{\sum_{ik} A_{ik} + Q_q}. \qquad (4)$$

Some more details on the LIF techniques and description of the used model can be found elsewhere [10, 15].

The potential of two-photon absorption laser-induced fluorescence spectroscopy for the spatially resolved determination of atomic oxygen densities at atmospheric pressure has recently been demonstrated for an APPJ [16, 17], being in good agreement with theoretical models for the oxygen chemistry of the effluent [18]. In contrast to the LIF, the TALIF technique is based on a two-photon absorption process in which the ground state $\langle 1\rangle$ is excited to an energetically higher state $\langle 3\rangle$ by simultaneous absorption of two photons

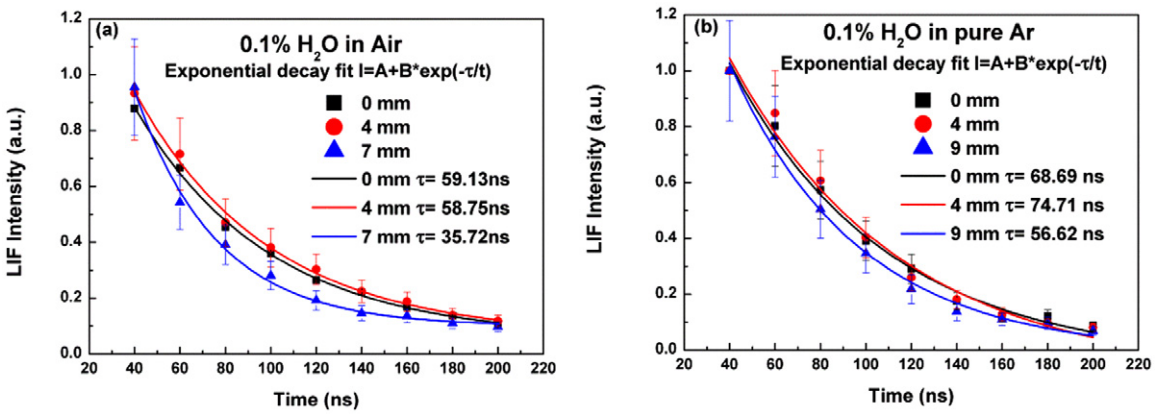


**Figure 3.** Time-resolved OH LIF signal intensity at different distances from the capillary nozzle after the laser pulse for the discharge in (*a*) air and (*b*) pure Ar. The systematic error of the measurements is about 18% and is determined by the experimental error in the measurements of the LIF signal. The offset of the LIF signal due to ICCD noise is (*a*) 0.1 and (*b*) 0.04, respectively.

through a virtual intermediate state $\langle i \rangle$. The total number of generated fluorescence photons $n_f$ can be written as

$$n_f = A_{32} \int_V \int_t n_3(t)\,dt\,dV = n_1 \frac{A_{32}}{A_3 + Q_3} \int_V \int_t R_{13}\,dt\,dV \quad (5)$$

where $A_3 = \sum_{i<3} A_{3i} g_{3i}$ denotes the total transition probability of the excited state $\langle 3 \rangle$, $Q_3 = \sum_q k_q^{(3)} n_q$ is the effective quenching rate induced by various collision partners with densities $n_q$, and $R_{13}$ is the two-photon excitation rate. For a more detailed description of the TALIF method see [16, 19]. The following scheme has been considered in order to determine the fluorescence yield $\eta$ in different spatial positions of the afterglow.

(I) The air fraction at a given distance from the nozzle is estimated based on the measured decay time of the LIF signal. This approach is based on a fact that the decay time $\tau$ of excited OH($A$) radicals can be experimentally determined and compared with the simulated value, e.g. from LASKIN [20] with the variable density of colliders as an input parameter. The best fit between the measured and calculated values of the parameter $\tau$ gives the desired value of the air fraction.

(II) For a known density and quenching rate [20–24] of the main colliders, namely $H_2O$, Ar, $N_2$ and $O_2$, $\eta$ can be calculated. Here, the quenching rates of the $O^{3p}$ state are considered to be $5.9 \times 10^{-10}$ cm$^3$ s$^{-1}$ by $N_2$, $9.3 \times 10^{-10}$ cm$^3$ s$^{-1}$ by $O_2$ and $0.25 \times 10^{-10}$ cm$^3$ s$^{-1}$ by Ar [21]. Data for collisional quenching of OH($A$) and ro-vibrational dependent cross-sections can be found in [20, 22–24].

(III) This way, the spatial distribution of the LIF and TALIF signals measured in ambient air and Ar atmosphere can be recalculated in order to be directly proportional to the ground-state species density.

## 3. Results

Figure 3 represents the decay of the OH($A$) LIF signal after the laser excitation for different distances from the nozzle. The data are obtained by an integration of the entire cross-section of the LIF image (circle with a diameter of 2.5 mm) in different positions along the axis of the jet. The overall intensity of the LIF signal is almost twice as high when the jet is working in ambient air but presented data are used only for the calculation of the air mole fraction in the jet afterglow and correspondingly all results in figure 3 are normalized. The OH fluorescence after laser pumping decreases in a gradual exponential way in both ambient air and argon. An offset observed in figure 3 at a time of 200 ns where the LIF signal is almost negligible in air and also in Ar appears due to the dark current of the ICCD and is not subtracted in figure 3. In argon atmosphere, the decay time remains constant at about 60–70 ns along the jet axis, as shown in figure 3(*b*). On the other hand, the lifetime of OH($A$) decreases significantly in ambient air from 59 to 36 ns with the distance from the nozzle. This decrease is caused by additional quenching of OH($A$) by $N_2$ and $O_2$. The mole fraction of air calculated from figure 3 varies from 0.5% at the distance of 1 mm from the nozzle to 2.3% and 5% at distances of 5 mm and 9 mm, respectively. The obtained air mole fraction is used for the calculation of the scaling factors $\eta_{air}$ and $\eta_{Ar}$ for both LIF and TALIF signals.

### *3.1. Spatially resolved measurements of OH radicals in the jet afterglow*

Figure 4 shows the spatially integrated OH LIF signal in ambient air and in argon where the quenching effect of OH($A$) according to the procedure mentioned above is taken into consideration. The signal is obtained by an integration of the LIF signal over the plasma jet cross-section. The axial distribution of the LIF signal in open air is very similar to the one in argon. It displays a plateau up to a distance of 4 mm from the nozzle, depending on the water content. Next, the signal intensity exponentially decreases from its maximum with the distance. It is found that OH density directly related to the LIF signal intensity presented in figure 4 is higher in the case of plasma jet working in ambient air for all investigated mixtures. As shown in figure 4, in the case of 0.1% $H_2O$, the LIF signal declines from its maximum value of 110 counts observed at 4 mm away from the nozzle to the 38% of its maximum at

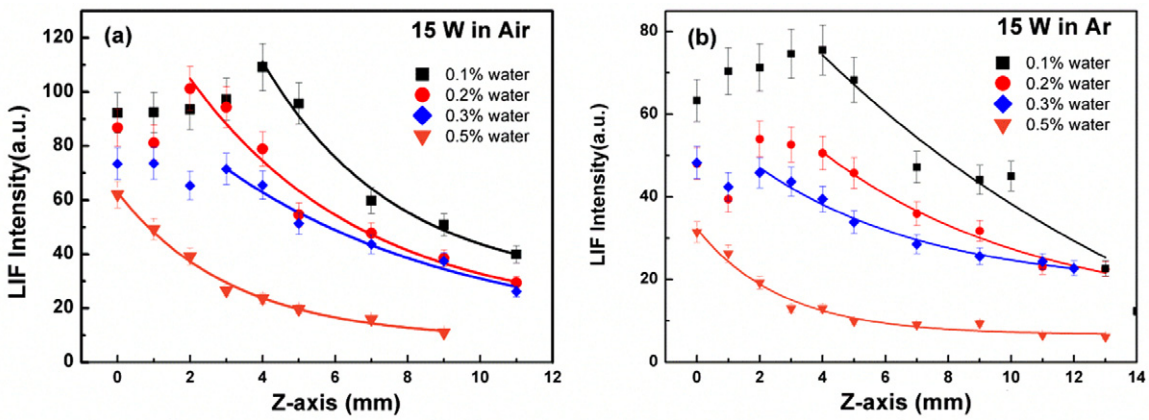


**Figure 4.** Spatial profile of OH LIF signals along the discharge axis, with (*a*) air and (*b*) pure argon as the ambient gas. The jet was operated at 15 W and 2 slm with a water admixture in argon varying from 0.1% to 0.5%.

**Table 1.** Most important reactions responsible for the loss of OH($X$) in the afterglow of the plasma jet.

| | Reactions | Rate constants | Ref |
|---|---|---|---|
| ($R_1$) | $OH + OH \longrightarrow H_2O + O$ | $6.2 \times 10^{-14}\,(298/T_g)^{2.6}\exp(945/T_g)$ cm$^3$ s$^{-1}$ | [25] |
| ($R_2$) | $OH + OH + Ar \longrightarrow H_2O_2 + Ar$ | $6.94 \times 10^{-31}$ cm$^6$ s$^{-1}$ | [25] |
| ($R_3$) | $Ar + H + OH \longrightarrow Ar + H_2O$ | $10^{-31}$ cm$^6$ s$^{-1}$ | [26] |
| ($R_4$) | $OH + O \longrightarrow O_2 + H$ | $2.4 \times 10^{-11}\exp(-109/T_g)$ cm$^3$ s$^{-1}$ | [27] |
| ($R_5$) | $OH + O_3 \longrightarrow HO_2 + O_2$ | $1.7 \times 10^{-12}\,(298/T_g)^2\exp(-945/T_g)$ cm$^3$ s$^{-1}$ | [25] |
| ($R_6$) | $OH + O_2 \longrightarrow HO_2 + O$ | $3.7 \times 10^{-11}\exp(-26\,506/T_g)$ cm$^3$ s$^{-1}$ | [25] |
| ($R_7$) | $OH + HNO \longrightarrow H_2O + NO$ | $8 \times 10^{-11}\exp(-500/T_g)$ cm$^3$ s$^{-1}$ | [28] |
| ($R_8$) | $OH + NO + Ar \longrightarrow HNO_2 + Ar$ | $7 \times 10^{-31}(T_g/298)^{-2.6}$ cm$^6$ s$^{-1}$ | [25] |
| ($R_9$) | $OH + NO_2 + Ar \longrightarrow HNO_3 + Ar$ | $2.5 \times 10^{-30}(T_g/298)^{-4.4}$ cm$^6$ s$^{-1}$ | [29] |

11 mm distance in air while the LIF signal in Ar gas decreases only to 67% from a value observed in the active discharge region at the same distance of 11 mm. Figure 4 illustrates that in air higher OH density is produced in the active discharge region and it diminishes rapidly in the post-discharge region. In general, the discharge afterglow can be divided into two zones: the active discharge region, characterized by almost constant LIF intensity, and the post-discharge region. As revealed by our previous measurements in open air [10, 15], the OH radical concentration is almost constant in the active zone with an order of magnitude of $10^{21}$ m$^{-3}$. Furthermore, OH radicals are transported forward to the post-discharge region where loss processes of OH($X$) become dominant. This is supported by the observed exponential decay of the OH LIF signal in this region. The OH concentration decreases along the axis mainly due to the fast recombination processes listed in table 1. The reactions ($R_5$)–($R_9$) are caused by air diffusion in the plasma. It explains why the LIF signal decreases faster in ambient air than in argon atmosphere.

In order to better understand the effect of air diffusion, a two-dimensional mapping of the LIF signal in open air and in the argon chamber is obtained and presented in figures 5 and 6. In the case of air as ambient gas, the LIF signal is concentrated in the vicinity of the central streamline, with a discharge diameter around 1.5 mm. In contrast to that, the discharge in ambient argon is approximately twice as broad, with a diameter of 3.0 mm at low water concentration. The maximum intensity of the OH LIF signal is approximately twice higher in the plasma working in open air than in the chamber filled with Ar. It is observed that the maximum of the OH density is located at a distance of about 2 mm from the nozzle in ambient air. The main mechanisms of OH($X$) production in this region in the Ar plasma with small addition of $H_2O$ are listed in table 2 and are electron impact reactions and reactions with Ar metastables [30, 31]. For the region with a low electron temperature, the water ion dissociative recombination can also play an important role in the production of OH radicals [32]. Admixing of $O_2$ into the jet due to air diffusion results in the quenching of Ar metastables and hence the reaction with metastables ($R_{11}$) cannot explain the observed higher density of OH($X$) radicals in the core of the jet when the jet works in ambient air. We expect that the main reason for OH enhancement in air is related to the change in electron density and electron temperature in the discharge in comparison with the case of the plasma generated in Ar environment. A more detailed investigation of the observed effect is presented in section 4.

### *3.2. Spatially resolved measurements of O atoms in the jet afterglow*

The experimentally observed temporal profile of the TALIF signal has the same shape as the laser pulse under all conditions, in contrast to the OH LIF signal having a decay time of 30–80 ns. The radiative decay time of the $O^{3p}$ level is 35 ns and it is reduced to 5 ns because of quenching by Ar alone. At atmospheric pressure, such a fast decay attributed to quenching by $O_2$ and $N_2$ has also been observed by many other groups,

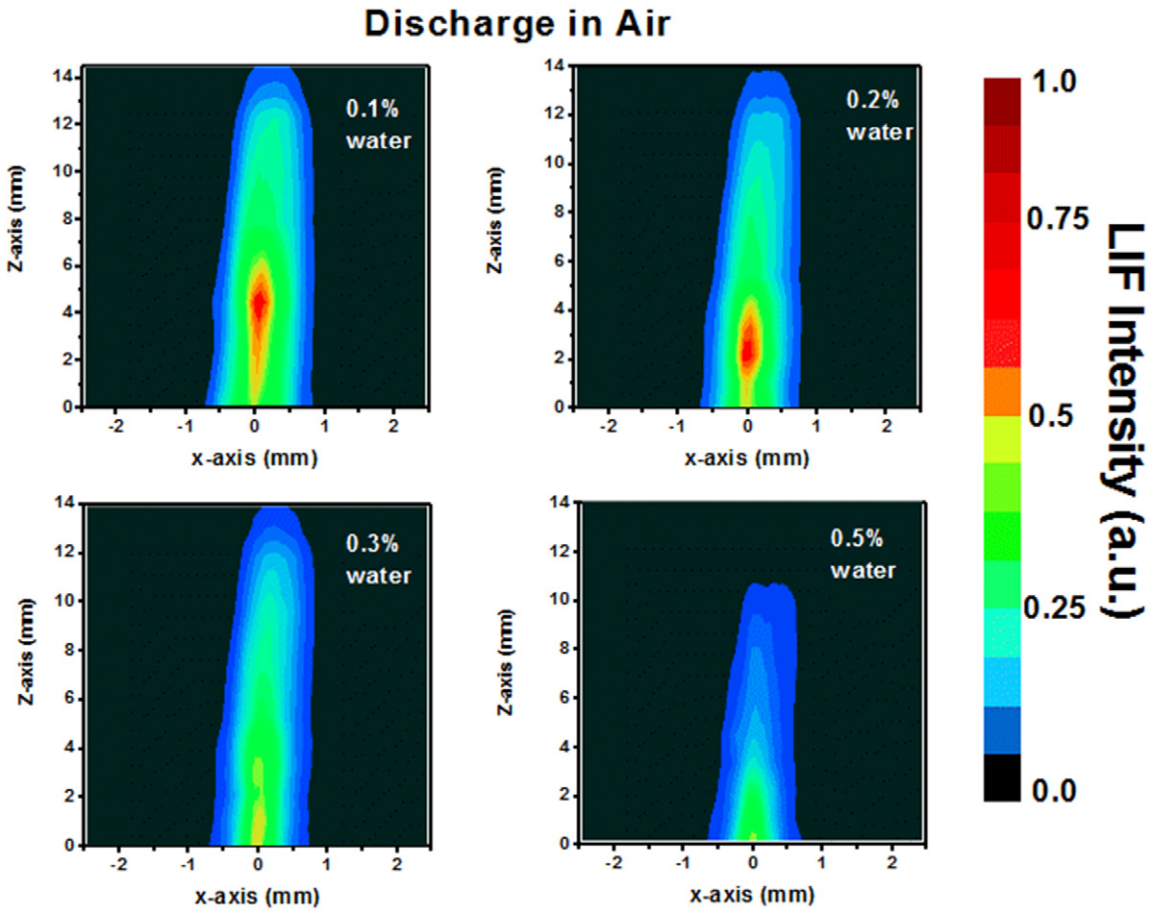


**Figure 5.** OH LIF signal maps in the plasma jet operated in ambient air with different water content.

e.g. in a coaxial microwave jet with a mixture of He and a few per cent of air [33]. Correspondingly, the time-resolved profile of TALIF has to follow the shape of the exciting laser pulse, whereas the intensity of the TALIF signal still strongly depends on the concentration of the quenchers, see equation (5). The cross-section-integrated TALIF signal of the jet in ambient air and inside the chamber has been measured under the same operating conditions as used for OH radicals. Figure 7 shows the spatially integrated TALIF signal for 0.3% and 0.5% addition of $O_2$ to the feed gas. The decrease in atomic O concentration again follows two modes in the discharge afterglow when it operates in argon: first the density of O decreases slowly up to 5 mm from the nozzle (figure 7(*b*) 0.5% $O_2$) and afterwards it drops exponentially. On the other hand, in ambient air, the atomic oxygen density just outside the nozzle exponentially falls off over a distance of a few millimeters. The same phenomenon has also been observed in a helium/oxygen RF plasma jet operated in open air by others [34]. We suggest that in a pure argon discharge, atomic O is generated in the first region due to dissociation of $O_2$ by electron impact and that recombination processes start to be dominant over O generation in the post-discharge region. The most important recombination reactions of atomic O are presented in table 3. In ambient air, reactions ($R_{14}$) and ($R_{16}$) start to be dominant in the post-discharge region where a high density of $O_2$ appears due to air diffusion. Additionally, atomic O recombines through effective three-body reactions with $N_2$ similar to processes ($R_{14}$) and ($R_{16}$) with almost the same rate constants [38, 39]:

$$(R_{18}):\ O + O_2 + N_2 \longrightarrow O_3 + N_2$$
$$k \approx 2.88 \times 10^{-33}\,\mathrm{cm^6\,s^{-1}}, \qquad T_g \approx 300\,\mathrm{K}$$
$$(R_{19}):\ O + O + N_2 \longrightarrow O_2 + N_2,$$
$$k \approx 2.56 \times 10^{-33}\,\mathrm{cm^6\,s^{-1}}, \qquad T_g \approx 300\,\mathrm{K}.$$

This explains the faster decay of the O signal in the afterglow in air. The 2D distribution of atomic O is presented in figure 8. The zone of O generation in the argon chamber is prolonged along the discharge axis to almost 12 mm (admixture of 0.5% $O_2$), in contrast to 7.5 mm in ambient air. However, a higher maximum intensity of the TALIF signal is observed in ambient air, which is almost thrice as high as that inside the chamber filled with Ar. The observed effect of air diffusion on the O distribution is similar to the case of OH radicals presented in figure 5. As a conclusion, air diffusion in to the discharge plays an important role in the production of active species and leads to an increase in their concentration in the discharge core for both mixtures of Ar/$H_2O$ and Ar/$O_2$.

## 4. Discussion

For both gas mixtures, the admixture of electronegative gas ($H_2O$ vapor or $O_2$) higher than 0.3% limits the production

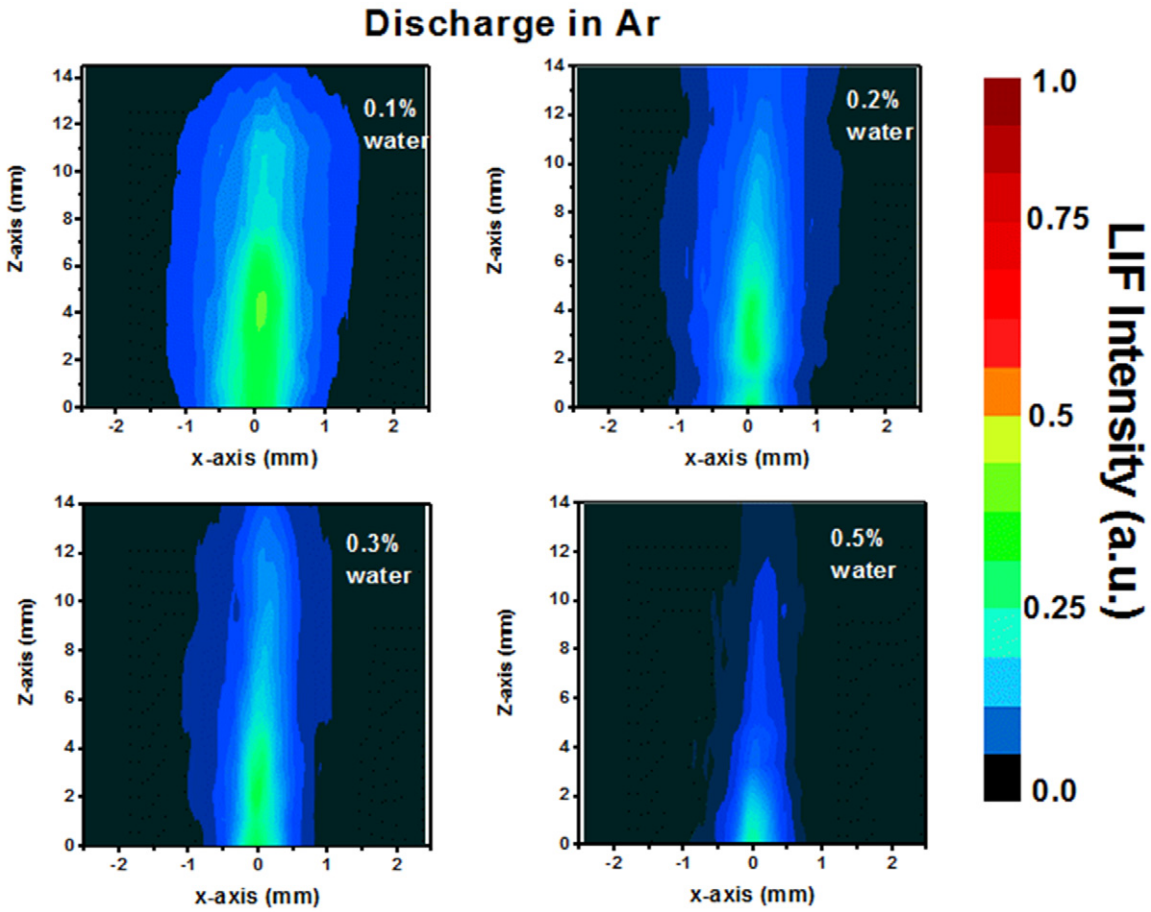


**Figure 6.** OH LIF signal maps in the plasma jet operated in ambient argon with different water content.

**Table 2.** Most important reactions responsible for the production of OH($X$) in ambient argon.

| | Reactions | Rate constants | Ref |
|---|---|---|---|
| ($R_{10}$) | $e^- + H_2O \rightarrow OH + H + e$ | $10^{-12}$–$10^{-10}$ cm$^3$ s$^{-1}$ ($T_e$ = 1–2 eV) | [30] |
| ($R_{11}$) | $Ar^m + H_2O \rightarrow OH + H + Ar$ | $4.5 \times 10^{-10}$ cm$^3$ s$^{-1}$ | [31] |
| ($R_{12}$) | $e^- + H_2O^+ \rightarrow OH + H$ | $2.6 \times 10^{-8} T_e^{0.5}$ cm$^3$ s$^{-1}$ | [32] |

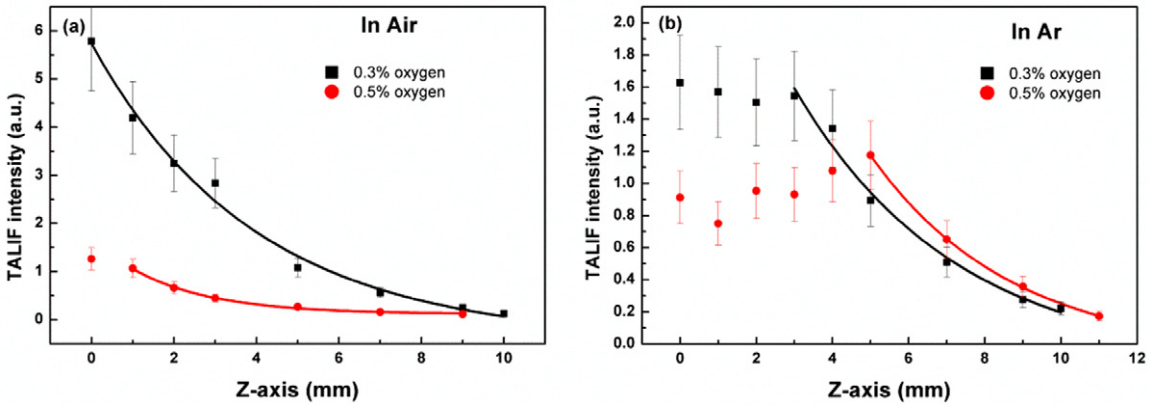


**Figure 7.** Spatial profile of the integrated O TALIF signals along the discharge axis, with ($a$) air and ($b$) pure argon as the ambient gas. The jet was operated at 15 W.

of the active species to only the core of the discharge. The expansion of the OH and O distribution is probably suppressed by fast reactions of OH radicals in the afterglow through mechanism ($R_2$) in the case of Ar/$H_2O$ mixture and by fast recombination of O with the formation of $O_3$ through reactions ($R_{13}$), ($R_{14}$) and ($R_{18}$) in the Ar/$O_2$ plasma. The noted higher densities of OH($X$) and O in the discharge in ambient air is an interesting phenomenon, which can be explained by changes

**Table 3.** Reaction rates of recombination processes involving atomic O in the afterglow of the Ar plasma jet.

| | Reactions | Rate constants | Ref |
|---|---|---|---|
| ($R_{13}$) | $O + O_2 + Ar \longrightarrow O_3 + Ar$ | $5.7 \times 10^{-34}(T_g/298)^{-2.6}$ cm$^6$ s$^{-1}$ | [25] |
| ($R_{14}$) | $O + O_2 + O_2 \longrightarrow O_3 + O_2$ | $7.3 \times 10^{-25}$ cm$^3$ s$^{-1}$ | [35] |
| ($R_{15}$) | $O + O + Ar \longrightarrow O_2 + Ar$ | $1.1 \times 10^{-34}\exp(-530/T_g)$ cm$^6$ s$^{-1}$ | [36] |
| ($R_{16}$) | $O + O + O_2 \longrightarrow O_2 + O_2$ | $2.56 \times 10^{-34}\ (300/T_g)^{0.63}$ cm$^6$ s$^{-1}$ | [37] |
| ($R_{17}$) | $O + O_3 \longrightarrow O_2 + O_2$ | $1.5 \times 10^{-11}\exp(-2250/T_g)$ cm$^3$ s$^{-1}$ | [18] |

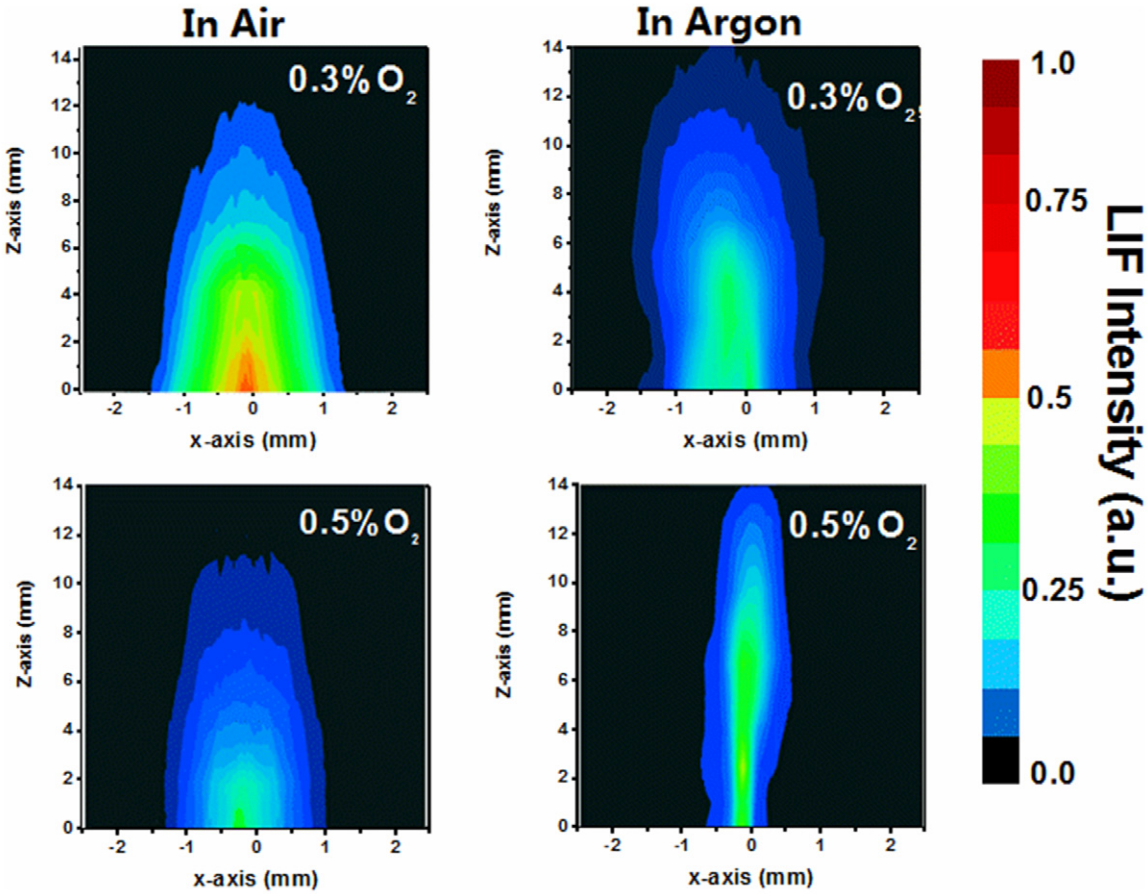


**Figure 8.** Spatially resolved TALIF signal of atomic O in the plasma jet operated in ambient air and in the argon chamber at different admixtures of $O_2$ in the feed gas.

in the chemical pathway of active species production or by a change in the plasma properties. In spite of the fast velocity of the feed gas of 10.6 m s$^{-1}$ at a gas flow of 2 slm, backward diffusion of air into the nozzle is still possible and can lead to a change in the gas phase composition and species density. We have found that the space-integrated air mole fraction is about 0.5% at a distance of 1 mm from the nozzle, but a small amount of impurities is also observed inside the nozzle during jet operation in open air. Figure 9 shows the emission spectrum of the discharge recorded by an Ocean Optics S2000 spectrometer with a 100 $\mu$m slit in front of the optical fiber. The intensity of the $N_2(C–B)$ band around 320–380 nm is strongly dependent on the position in the afterglow and has the highest intensity at a distance of 5 mm from the nozzle where the air mole fraction reaches ~2.5%. The $N_2(C–B)$ emission is still detectable at 1 mm from the nozzle and even inside the quartz capillary. This means that the influence of air impurities on the production of active species in the core of the plasma has to be considered. Komuro *et al* [40] found that dissociation of $H_2O$ by $O(^1D)$ and $N_2(A)$ is predominant in the production of OH in a streamer discharge in humid air. In that case, the following mechanisms can lead to additional formation of OH radicals in the afterglow [25, 41]:

$$(R_{20}):\ O(^1D) + H_2O \rightarrow OH + OH$$

$$(R_{21}):\ \Sigma N_2\left(A^3_{u^+}\right) + H_2O \rightarrow N_2 + OH + H,$$

$$k = 6 \times 10^{-14}\ \text{cm}^3\ \text{s}^{-1}, \qquad T_g \approx 300\ \text{K}.$$

The reaction rate with $O(^1D)$ for OH production is much higher than those of electron or metastable dissociation of $H_2O$ [40] and thus enhances OH production in the afterglow of the plasma jet in ambient air. Similar to reaction ($R_{21}$), a mechanism has been proposed in [41] for the generation of O:

$$(R_{22}):\ \Sigma N_2\left(A^3_{u^+}\right) + O_2 \rightarrow N_2 + O + O,$$

$$k = 2 \times 10^{-11}\ \text{cm}^3\ \text{s}^{-1}.$$

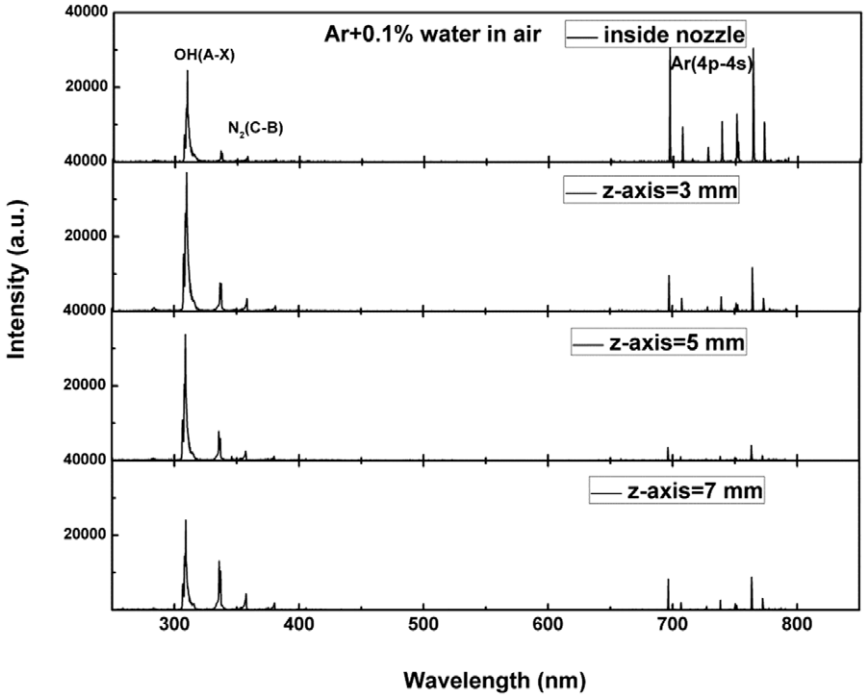


**Figure 9.** Spatially resolved emission spectrum of the plasma jet working at 2 slm and a power of 15 W. The spatial resolution of the system is 1 mm.

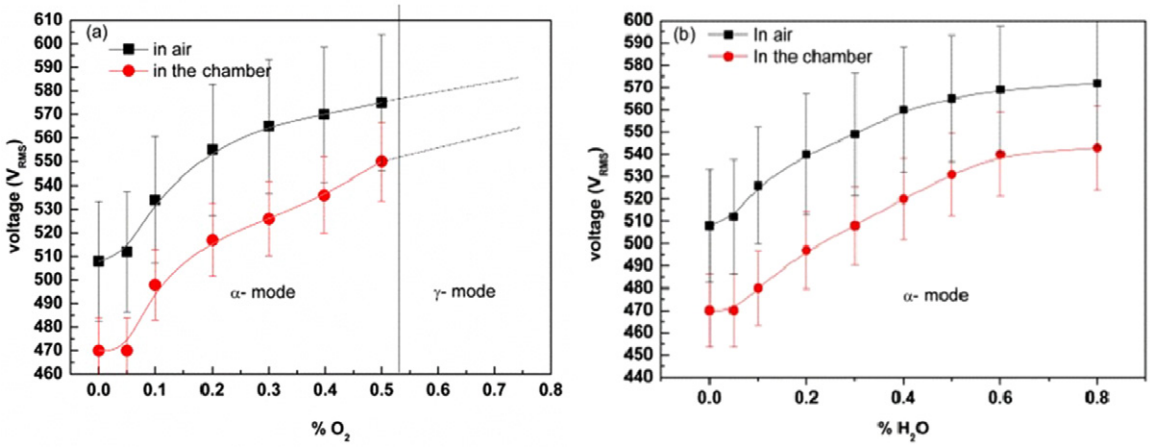


**Figure 10.** Operational voltage as a function of $O_2$/$H_2O$ admixture in the feed gas for the plasma jet working in open air and inside the argon chamber.

However, because of air diffusion into the jet, the active species map has to follow a 'donut'-like distribution, with higher intensity on the edges, due to the profile of $N_2$, $H_2O$ and $O_2$ densities in the afterglow. In fact, the 'donut'-like shape of the LIF OH distribution in the afterglow of a He pulsed discharge operated in ambient air has been observed recently in [42]. The appearance of a central dip in the LIF signal after the discharge is also observed by Ono and Oda for a 100 Torr and a 760 Torr pulsed discharge [43]. They saw an expansion of the LIF signal on the time scale of tens of microseconds, and this was solely attributed to diffusion effects. A similar 'donut'-like distribution of OH radicals on time scales of 100 ns after a discharge pulse in an atmospheric filament discharge has been observed and explained by a higher temperature in the core and thus high depletion of OH through ionization [44]. It is contradictory with this study where the distribution of the OH and O species has almost a Gaussian profile with the maximum in the center of the plasma and 'donut'-like shape has not been observed. Therefore, only reactions ($R_{20}$)–($R_{22}$) cannot explain the higher concentration of OH and O for the case of the discharge in ambient air. On the other hand, the difference in 2D distributions of species can be observed because of the constriction of the discharge and higher density and temperature of electrons in the plasma in ambient air. Figure 10 displays the value of operation voltage for Ar/$H_2O$ and Ar/$O_2$ gas mixtures. The discharge in Ar/$O_2$ mixtures tends to transfer from $\alpha$-mode to $\gamma$-mode at a high value of $O_2$admixture and thus, no data are presented for $O_2$ concentration higher than 0.5%. A voltage of 470 $V_{RMS}$ is required to sustain the discharge in argon, while

about 510 $V_{RMS}$ is needed when the plasma jet is working in ambient air. The difference of 40 ± 10 $V_{RMS}$ in discharge voltage is registered for all used conditions. A similar effect has been observed by Sun and co-workers [45] for an RF discharge between two copper electrodes with He as the feed gas. The higher breakdown and operation voltage needed for discharge ignition and sustaining results in a higher electrical field in the plasma and a higher electron density $N_e$, and probably electron temperature. Such an increase in $N_e$ will lead to a higher yield of OH and O due to electron impact dissociation of $H_2O$ and $O_2$, and can explain the observed enhancement of active species during operation of the jet in ambient air.

## 5. Conclusion

The effect of air admixture on active species production and distribution in an atmospheric-pressure plasma jet is investigated. Laser-induced fluorescence spectrometry is used for measurements of the spatial distribution of OH radicals and atomic O in the plasma jet, both in ambient air and in a chamber with controlled argon atmosphere. Additionally, the admixture of air into the plasma effluent is quantified to be 0.5% at a distance of 1 mm from the nozzle to 2.3% and 5% at distances of 5 mm and 9 mm, respectively, based on the measured decay time of the LIF signal.

The admixture of air into the effluent leads to a shorter propagation distance of the OH radicals and O atoms out of the jet's nozzle. This is mainly because of the fast recombination processes of OH and O with intrusions of nitrogen and oxygen molecules from the surrounding air environment. A higher yield of OH and O is observed in the core of the discharge when the discharge is operated in ambient air. It is explained by a higher operation voltage, with a difference of 40±10 $V_{RMS}$ for all used conditions, required to sustain the discharge in air. Based on the measurement of the discharge voltage in different atmospheres, the higher detected density of active species in the discharge in ambient air is likely due to the higher electron density and more effective electron impact dissociation of $H_2O$ and $O_2$.

## Acknowledgments

This work is supported by the Interuniversity Attraction Poles Program of the Belgian Science Policy (Project 'PSI'-P6/08), partially supported by FWO grant 1.5.005.13N, by the China Scholarship Council (CSC), and NB is a postdoc researcher of the FNRS Belgium.

## References

[1] Kunhardt E E 2000 *IEEE Trans. Plasma Sci.* **28** 189
[2] Kogelschatz U 2002 *IEEE Trans. Plasma Sci.* **30** 1400
[3] Stalder K R, Nersisyan G and Graham W G 2006 *J. Phys. D. Appl. Phys.* **39** 3457
[4] Blakely E A, Bjornstad K A, Galvin J E, Monteiro O R and Brown I G 2002 *IEEE Int. Conf. on Plasma Science (Banff, Canada, 26–30 May 2002)* vol 253
[5] Sanchez-Estrada F S, Qiu H and Timmons R B 2002 *IEEE Int. Conf. on Plasma Science (Banff, Canada, 26–30 May 2002)* vol 254
[6] Yanguas Gil A, Focke K, Benedikt J and von Keudell A 2007 *J. Appl. Phys.* **101** 103307
[7] Foest R, Kindel E, Ohl A, Stieber M and Weltmann K D 2005 *Plasma Phys. Control. Fusion* **47** B525–36
[8] Nikiforov A, Xiong Q, Britun N, Snyders R, Lu X P and Leys C 2011 *Appl. Phys. Express* **4** 026102
[9] Nikiforov A, Li L, Xiong Q, Leys C and Lu X P 2011 *Eur. Phys. J. Appl. Phys.* **56** 24009
[10] Xiong Q, Nikiforov A, Li L, Britun N, Snyders R, Lu X P and Leys C 2012 *Eur. Phys. J.* D **66** 281
[11] Li L, Nikiforov A, Xiong Q, Lu X P, Taghizadeh L and Leys C 2012 *J. Phys. D: Appl. Phys.* **45** 125201
[12] Crosley D R and Lengel R K 1975 *J. Quantum Spectrosc. Radiat. Transfer* **15** 579
[13] Ono R, Yamashita Y, Takezawa K and Oda T 2005 *J. Phys. D: Appl. Phys.* **38** 2812
[14] Ono R and Oda T 2008 *Combust. Flame* **152** 69–79
[15] Li L, Nikiforov A, Xiong Q, Lu X P, Taghizadeh L and Leys C 2013 *Phys. Plasmas* **20** 093502
[16] Niemi K, Schulz-von der Gathen V and Dobele H F 2005 *Plasma Sources Sci. Technol.* **14** 375
[17] Knake N, Reuter S, Niemi K, Schulz-von der Gathen V and Winter J 2008 *J. Phys. D: Appl. Phys.* **41** 194006
[18] Jeong J Y *et al* 2000 *J. Phys. Chem.* A **104** 8027
[19] Dobele H F, Mosbach T, Niemi K and Schulz-von der Gathen V 2005 *Plasma Sources Sci. Technol.* **14** S31
[20] Rahmann U, Bulter A, Lenhard U, Dusing R, Markus D, Brockhinke A and Kohse-Hoinghaus K 2003 LASKIN—a simulation program for time-resolved LIF-spectra *Internal Report* University of Bielefeld, Faculty of Chemistry, Physical Chemistry
[21] Niemi K, Schultz-von der Gathen V and Dobele H F 2001 *J. Phys. D: Appl. Phys.* **34** 2330–5
[22] Wysong I J, Jeffries J B and Crosley D R 1990 *J. Chem. Phys.* **92** 5218
[23] Williams L R and Crosley D R 1996 *J. Chem. Phys.* **104** 6507
[24] Kienle R, Lee M P and Hoinghaus K 1996 *Appl. Phys.* B **62** 583–99
[25] Atkinson R, Baulch D L, Cox R A, Crowley J N, Hampson R F, Hynes R G, Jenkin M E, Rossi J M and Troe J 2004 *Atmos. Chem. Phys.* **4** 1461–738
[26] Sellevag S R, Georgievskii Y and Miller J A 2008 *J. Phys. Chem.* A **112** 5085–95
[27] Herron J T and Green D S 2001 *Plasma Chem. Plasma Process.* **21** 459–81
[28] Tsang W and Herron J T 1991 *J. Phys. Chem. Ref. Data* **20** 609–63
[29] DeMore W B, Sander S P, Golden D M, Hampson R F, Kurylo M J, Howard C J, Ravishankara A R, Kolb C E and Molina M J 1997 *JPL Publication* vol 97-4, pp 1–266
[30] Itikawa Y and Mason N 2005 *J. Phys. Chem. Ref. Data* **34** 1–22
[31] Novick S and Krenos J 1988 *J. Chem. Phys.* **89** 7031
[32] Jensen M J, Bilodeau R C, Heber O, Pedersen H B, Safvan C P, Urbain X, Zajfman D and Andersen L H 1999 *Phys. Rev.* A **60** 2970–6
[33] van Gessel A F H, van Grootel S C and Bruggeman P 2013 *Plasma Sources Sci. Technol.* **22** 055010
[34] Schroder D, Bahre H, Knake N, Winter J, de los Arcos T and Schulz-von der Gathen V 2012 *Plasma Sources Sci. Technol.* **21** 024007
[35] Castellano E and Schumacher H J 1962 *Z. Phys. Chem. (Neue Folge)* **34** 198–212

[36] Naudet V, Abid S and Paillard C E 1999 *J. Chem. Phys.* **96** 1123–45
[37] Stafford D S and Kushner M J 2004 *J. Appl. Phys.* **96** 2451
[38] Gross A, Barnes I, Sorensen R M, Kongsted J and Mikkelsen K V 2004 *J. Phys. Chem.* A **108** 8659–71
[39] Smith G P and Robertson R 2008 *Chem. Phys. Lett.* **458** 6–10
[40] Komuro A, Ono R and Oda T 2013 *J. Phys. D: Appl. Phys.* **46** 175206
[41] Herron J T 1999 *J. Phys. Chem. Ref. Data* **28** 1453–83
[42] Pei X, Lu Y, Wu S, Xiong Q and Lu X 2013 *Plasma Sources Sci. Technol.* **22** 025023
[43] Ono R and Oda T 2001 *IEEE Trans. Indust. Appl.* **37** 709–14
[44] Verreycken T, van der Horst R M, Baede A H F M, van Veldhuizen E M and Bruggeman P 2012 *J. Phys. D: Appl. Phys.* **45** 045205
[45] Li G, Li H, Wang L, Wang S, Zhao H, Sun W, Xin X and Bao C 2008 *Appl. Phys. Lett.* **92** 221504